

# INVESTIGATION OF THE IMPACT OF SPEED-RIPPLE AND INERTIA ON THE STEADY-STATE CURRENT SPECTRUM OF A DFIG WITH UNBALANCED ROTOR

*S. Djurović\**, *S. Williamson*<sup>†</sup>

*\*School of Electrical and Electronic Engineering, The University of Manchester, Manchester M60 1QD, UK*

*<sup>†</sup>University of Surrey, Guildford, Surrey GU2 7XH, UK*

*e-mail: Sinisa.Durovic@manchester.ac.uk, Steve.Williamson@surrey.ac.uk*

**Keywords:** DFIG, Unbalanced rotor, Current Spectrum, Speed Ripple, Inertia

## Abstract

This paper investigates the influence of speed ripple and effective rotational inertia on the stator current harmonic content of a DFIG operating with a rotor electrical unbalance. For this purpose a time-stepped numeric DFIG model is employed. A model study is performed for a range of operating scenarios of interest. The effect of different types of rotor unbalance (supply/windings) on the stator current spectrum is also examined.

## 1 Introduction

Doubly fed induction generator (DFIG) remains one of the preferred drive system options for contemporary MW scale variable speed wind turbines. This is mainly due to the advantages that DFIGs offer in terms of optimized power production and reactive power flow manipulation. DFIGs are now vital elements of remote and difficult to access wind farm systems and therefore the early detection of potential defects in these machines is essential in order to avoid supply outages and minimize costly repairs.

In an attempt to provide a reliable and efficient fault detection tool a number of authors have performed frequency domain analysis of DFIG current [1-5]. The aim was to identify potential fault-specific harmonic signatures for a range of stator and rotor electric faults. When cage rotor induction machine rotor asymmetry detection is concerned the traditional approach in this context is based on identifying the presence of sidebands in the stator current spectrum at  $(1 \pm 2s)f$  Hz, where  $s$  is the fractional slip and  $f$  the supply frequency [6,7]. The manner in which these sidebands are manifested in cage rotor machine current is known to be strongly influenced by factors such as speed ripple and rotational inertia [8,9]. DFIG rotor electric fault detection algorithms based on the existence of the aforementioned components in the faulty generator current spectrum were also proposed recently [4]. However, when grid connected DFIGs are concerned these sideband components may also arise during regular generator operation in unbalanced supply conditions. Their presence is also strongly affected in both wound and cage rotor machines by any inherent rotor unbalance originating from inevitable

manufacturing imperfections. The objective of this paper is to examine the harmonic content of steady-state DFIG stator current when generator is operating with unbalanced rotor windings or supply and to evaluate the influence of speed ripple and inertia on the manner of induction of sideband components in the current spectrum. This analysis is achieved by performing a study based on using a purpose devised DFIG analytical model. The presented work involves a range of DFIG operating scenarios where the influence of individual factors such as rotor supply or winding unbalance, speed ripple and inertia, on the DFIG steady state current frequency spectrum is evaluated in turn.

## 2 Generator Modelling

The basis for this work is a DFIG time-stepped numerical model that employs the concepts of harmonic winding analysis and coupled impedance approach [5]. The model consists of a standard set of induction machine electromechanical equations:

$$[V] = [R][I] + \frac{d[\Psi]}{dt} \quad (1)$$

$$[\Psi] = [L][I] \quad (2)$$

$$T_e - T_L = J \frac{d\omega}{dt} \quad (3)$$

where  $[V]$  is the machine voltage matrix,  $[R]$  is the machine resistance matrix,  $[I]$  is the machine current matrix,  $[\Psi]$  is the machine flux linkage matrix,  $[L]$  is the machine inductance matrix,  $T_e$  is the machine electromagnetic torque,  $T_L$  is the load torque,  $J$  is the combined rotor inertia and  $\omega$  is the rotor mechanical speed. Model equations also incorporate a connection matrix defined for the particular winding arrangement of interest, thus enabling the model calculations to accommodate various balanced/unbalanced winding configurations. The model is also capable of accounting for supply unbalance, since supply voltage is one of the necessary inputs for the numerical algorithm. In addition, higher order

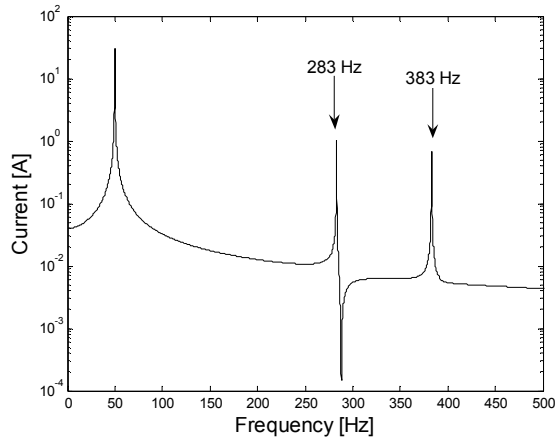
air-gap field harmonics are taken into account when evaluating model parameters thus making this model particularly suitable for frequency domain analysis of machine electrical quantities. Model equations are solved in an appropriate time-stepping numerical algorithm. The validity of this model has been extensively verified in both time and frequency domain against experimental data from a purpose-built DFIG test rig and its principles presented in [5,10-12].

### 3 Machine Current Spectrum Model Study for Balanced/Unbalanced Rotor Operation

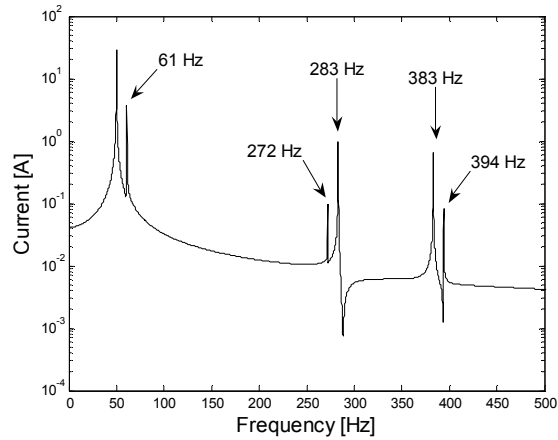
The described model was used to simulate DFIG operation. The data used in calculations are for an industrial four-pole 30 kW wound rotor induction machine. The results shown in this section are for an arbitrary typical super-synchronous steady-state speed of  $1665 \text{ rpm}$  and a constant load torque. Rotor and stator supply are modelled in calculations as single frequency sine waves, i.e. higher order supply harmonic voltages are neglected for the purpose of this study. Time domain simulation results for DFIG steady-state stator current were processed in MATLAB using the built-in FFT algorithm. These are shown in Fig. 1 for a range of operating scenarios.

The presented data are limited to a bandwidth of  $0-500 \text{ Hz}$ . The following cases are considered in the study:

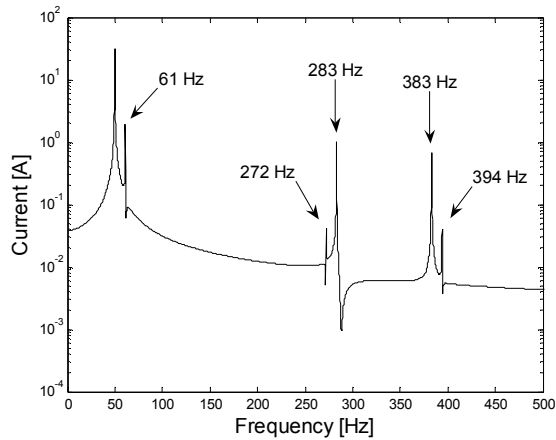
- a) Current spectrum shown in Fig. 1a is for operation with balanced supply and windings and with the rotor speed held constant. This is accomplished by following a procedure in which the mechanical speed is obtained in simulation by resolving the machine mechanical characteristic equation (3) in a series of iterative steps until a steady-state solution is achieved. Once the steady state operation is reached the rotational speed is held at that value in the simulation. The transition from varying to fixed speed is evident in the corresponding model results for speed, shown in Fig. 2. This procedure enables any effects caused by rotor speed fluctuations to be removed from the model results. Furthermore, when speed variation is reintroduced into the model it becomes possible to identify those harmonic components that are attributable to the fluctuation of the rotor speed. The results shown in Fig. 1a demonstrate that further to the fundamental  $50\text{Hz}$  component the constant speed DFIG steady-state spectrum also contains additional harmonic components at higher frequencies:  $283 \text{ Hz}$  and  $383 \text{ Hz}$  for the chosen operating speed. These frequency components are always present in a DFIG [5,10,11].
- b) The spectrum presented in Fig. 1b is for a DFIG operating



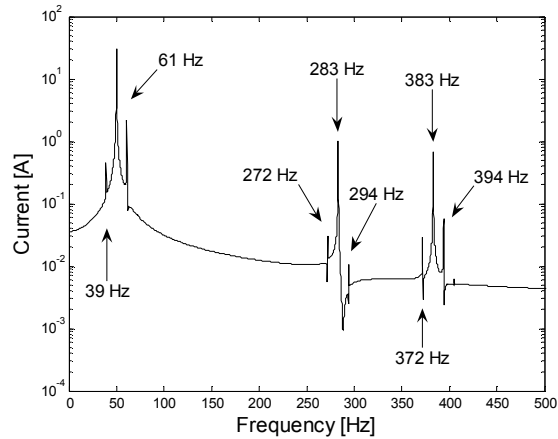
a) Balanced supply and windings, constant speed



b) Unbalanced rotor supply, constant speed



c) Unbalanced rotor windings, constant speed



d) Unbalanced rotor windings, speed allowed to fluctuate

Fig. 1 DFIG stator current FFT spectrum,  $1665 \text{ rpm}$

with balanced windings and stator supply, and a rotor supply unbalance. As before the rotor is assumed to rotate at constant speed. A 3% fundamental negative sequence rotor supply unbalance was introduced in the simulations. The results indicate that, when compared to balanced operation, this minor DFIG rotor supply unbalance will give rise to additional harmonic components in the current spectrum - these are the sidebands labelled in the graph at 61, 272 and 394 Hz.

c) The effect of a resistive rotor winding unbalance on the DFIG steady-state current spectrum is shown in model results in Fig. 1c. In this instance both stator and rotor supplies are assumed to be balanced and the speed is held constant, however a 20% resistive unbalance was introduced in one of the rotor phase windings. The calculated data show that winding unbalance also gives rise to additional components in the stator current spectrum, marked in Fig. 1c at 61, 272 and 394 Hz.

d) Lastly, in order to evaluate the influence of speed fluctuations, the DFIG mechanical characteristic was resolved for speed at each iteration step in the numerical algorithm, i.e. the ripple in the DFIG speed signal was allowed to affect the machine behaviour. Identical operating conditions to those modelled in c) were simulated and model results for current FFT spectrum are shown in Fig. 1d. It is evident that the speed ripple gives rise to additional sidebands in the current spectrum at 39, 294 and 372 Hz - these were not present in any of the previously considered cases.

Model results in Fig. 1 provide an overview of the effects that rotor winding and supply unbalance and the speed ripple individually have on DFIG steady-state stator current frequency content. Presented data indicate that these factors typically result in additional sideband components in the current spectrum. The authors have shown that all of the above discussed current harmonic frequencies are slip dependant and calculable [5].

The mechanism of induction of stator current sideband components that originate from rotor unbalance and speed ripple in standard cage rotor machines is well known [8,9]. The underlying premise here is, that the perfect symmetry, that is assumed to be characteristic of a healthy machine, is disturbed by a rotor electric asymmetry giving rise to rotor reverse rotating slip frequency air-gap field that results in  $(1-2s)f$  harmonic component in the primary current. This induced current now interacts with the stator flux and produces torque and consequently speed oscillations at double slip frequency. The resulting speed oscillation is manifested as an additional disturbance in the flux and produces stator emfs and their resulting currents at  $(1\pm 2s)f$  Hz. The upper sideband component at  $(1+2s)f$  Hz in conjunction with the existing rotor asymmetry gives rise to reverse rotating rotor field at  $3sf$  Hz and the induction process starts a new cycle. This series of induction cycles results in a sequence of sideband components. In the cage rotor machine stator current these may exist at  $(1\pm 2ns)f$  Hz, where  $n = 1, 2, 3, \dots$ . The described induction mechanism is heavily influenced by rotational inertia that directly affects the speed fluctuations, and also by the level of unbalance present on the rotor.

The above described principles also hold true for wound rotor

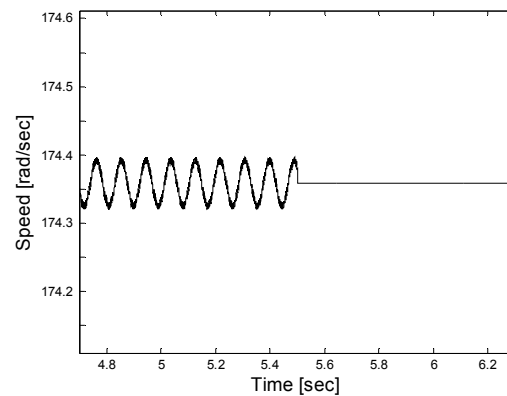


Fig. 2 Steady-state speed signal: calculated ( $t < 5.5$  sec) and held constant ( $t > 5.5$  sec)

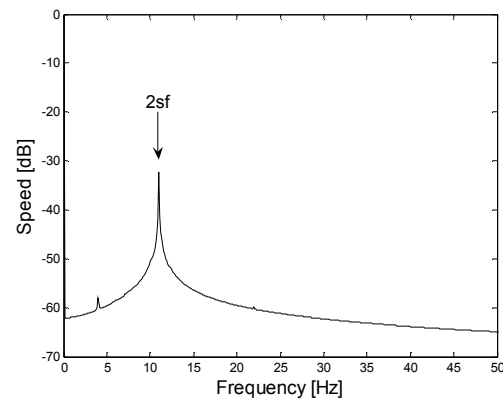


Fig. 3 Calculated speed FFT spectrum, case d)

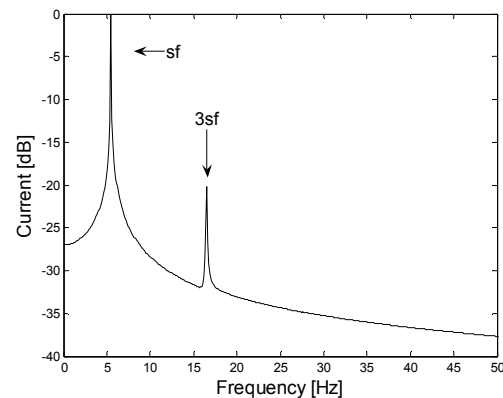


Fig. 4 Calculated rotor current FFT spectrum, case d)

induction machines such as DFIGs. This is illustrated by model results shown in Fig. 3 and 4 for DFIG speed and rotor current FFT spectrum, corresponding to the operating scenario considered in study case d). The data are normalized with respect to the dominant component and limited to a bandwidth of 0-50 Hz. The DFIG speed signal spectrum in Fig. 3 is seen to contain a  $2sf$  component resulting from the introduced rotor unbalance. The effect of this first harmonic of speed ripple in the rotor current in Fig. 4 is demonstrated as a  $3sf$  component. The corresponding stator current spectrum in Fig. 1d is seen to contain the  $(1\pm 2s)f$  components

(i.e. 39 and 61 Hz for the chosen operating speed). Higher order sidebands around the fundamental are not seen at this level of rotor unbalance and inertia. More importantly, the data in Fig. 1d demonstrate the presence of a number of sideband components at higher frequencies, namely those at 272, 294, 372 and 394 Hz - these are also caused by the rotor unbalance.

The manner in which the rotor unbalance induced sidebands around the fundamental component are manifested in the DFIG stator current is shown here to be consistent with their counterparts found in cage rotor machine primary current. It was shown in [5,10,11] that, due to their construction features, wound rotor induction machines contain harmonic rich air-gap fields that result in well defined higher order components in the stator current spectrum. Compared to cage rotor machines the considered rotor asymmetry induced sidebands in DFIG stator current are therefore substantially different in that they are also extended to higher frequencies found in the balanced machine current spectrum. Study results in Fig. 1a for an ideal case when the machine is perfectly balanced and operating with no speed fluctuation clearly show the higher order harmonic content of the DFIG stator current. In terms of the rotor asymmetry effect on the stator current, these higher frequency components will act equivalently to the fundamental, that is they will present "carriers" for the sideband components to be induced on. The mechanism of induction will be identical to that previously described, where the primary effect of a rotor electrical unbalance will be to induce the  $-2sf$  sideband component on each of the three "carriers" shown in the spectrum (i.e. the fundamental 50 Hz, and 283 Hz and 383 Hz for the chosen operating speed). This is clearly illustrated in model results in Figs. 1b-d. The data in Figs. 1b-d also show that these  $-2sf$  sidebands appear at "opposite" sides of higher frequency components, i.e. at 272 and 394 Hz. This can be explained by the fact that the air-gap fields that relate to 283 and 383 Hz components in the stator current rotate in opposite directions, i.e. the 283 Hz field is reverse rotating and the 383 Hz rotates in the forward direction [5]. Finally, the speed fluctuations will yield the  $+2sf$  sidebands on 50, 283 and 383 Hz, which are seen to be manifested in the current spectrum in the manner consistent to their  $-2sf$  counterparts. In addition, any supply introduced higher order harmonics in the DFIG current spectrum at integer multiples of the fundamental 50 Hz frequency will also provide a carrier frequency for unbalance and speed ripple induced sideband components. These effects are not illustrated here as higher order supply harmonics are neglected in this work.

Results in Fig. 1 also indicate that, although the rotor supply unbalance and the rotor winding unbalance in DFIGs originate from a different source, they will induce identical harmonic signatures in the stator current in terms of the present harmonic frequencies. This is for a simple reason that both these asymmetries will have the same effect on the rotor fields, i.e. they will both result in reverse rotating field components. The rotor winding unbalance considered here is purely resistive and as such is more representative of an inherent asymmetry or a brush-gear disturbance; the effects of a different type of rotor winding unbalance such as a

short/open circuit fault would be much less linear due to the fact that it is the whole winding impedance that changes in case of fault and not only its resistive part. This would affect the coupling of electric circuits within the machine and consequently the air gap flux distribution in a more profound manner and depending on the machine design features may yield different results for the stator current spectrum content [5].

#### 4 Influence of rotor unbalance severity and rotational inertia

The impact of the level of DFIG rotor electric unbalance and rotational inertia on the induced sideband components in the primary current is examined and quantified in this section. For this purpose a series of simulations were undertaken, where in the first instance various degrees of winding and supply unbalance are introduced in the rotor circuit. The analysis then moves on to considering the influence of inertia value on the unbalanced machine primary current spectrum. Rotor speed fluctuation is included in model calculations throughout the analysis. The data presented are normalized with respect to the dominant component in their respective spectra and limited to a bandwidth of 0-500 Hz for stator current and 0-50 Hz for rotor current and speed. The results are shown for a simulated identical operating speed and loading conditions to those used previously in this work.

Results in Fig. 5-6 are for an introduced rotor resistive unbalance in the model. Further to the data in Fig. 1d, two different arbitrary unbalance levels are considered here for illustrational purposes. First, a resistive unbalance involving the addition of 50% of the rotor total phase resistance to one of the rotor phase windings was introduced in the simulations; then a more severe unbalance of 150% was simulated. Corresponding model results for stator current FFT spectrum are shown in Fig. 5 and 6, respectively. The introduced rotor resistive unbalance is seen to follow the previously identified pattern of behavior in terms of the induced asymmetry-specific sideband components in the spectrum. It can also be observed that, as the level of the introduced rotor asymmetry progresses so do the magnitude and the number of the induced sideband components throughout the spectrum. The sideband frequencies are labeled in the graphs. Model results for simulated rotor voltage supply unbalance follow the same principles. Two supply asymmetry levels are investigated, where first a 5% fundamental negative sequence rotor supply unbalance was introduced in the simulations and then the unbalance level was raised to 15%. The corresponding calculated stator current spectra are shown in Fig. 7 and 8, respectively. The data in Fig. 5-8 demonstrate a consistent stator current spectrum reaction to different rotor unbalance levels despite the fact that different types of electric asymmetry were introduced on the rotor. As was mentioned in the previous section, this is because the fundamental rotor asymmetry induced effect is identical, i.e. a winding or a supply unbalance will both give rise to reverse rotating slip frequency field components. The number/magnitude of detectable sideband components is seen here to be directly related to the degree of induced field unbalance, which in turn

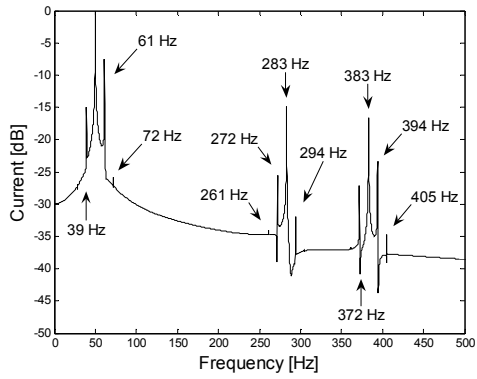


Fig. 5 Stator current FFT: 50% resistive unbalance, 1665 rpm

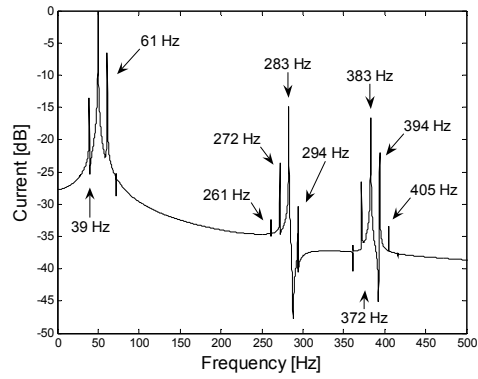


Fig. 7 Stator current FFT: 5% supply unbalance, 1665 rpm

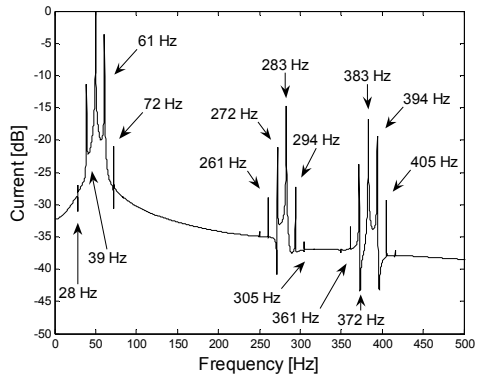


Fig. 6 Stator current FFT: 150% resistive unbalance, 1665 rpm

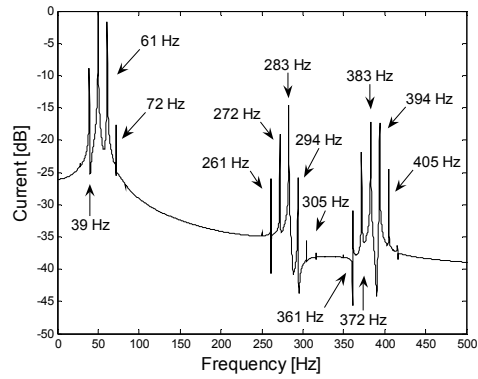


Fig. 8 Stator current FFT: 15% supply unbalance, 1665 rpm

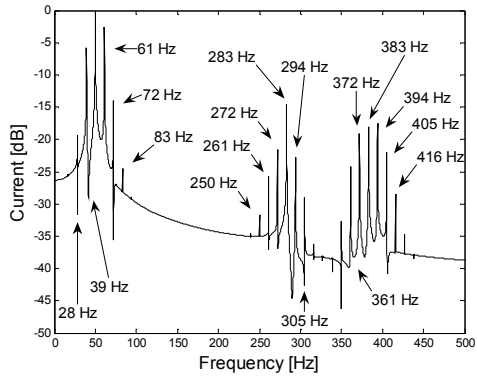


Fig. 9 Stator current FFT: 50% resistive unbalance,  $J/2$ , 1665 rpm

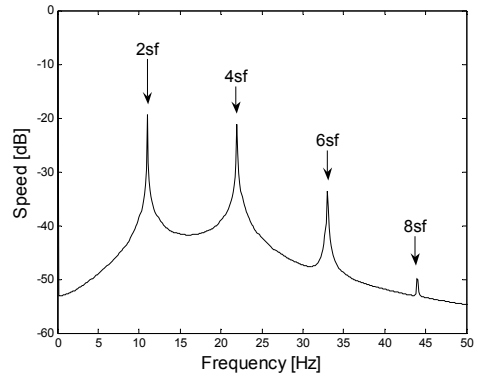


Fig. 11 Speed FFT: 50% resistive unbalance,  $J/10$ , 1665 rpm

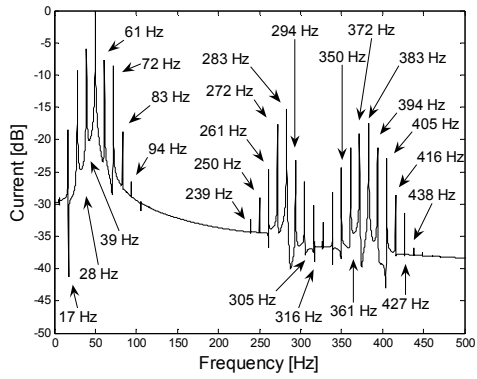


Fig. 10 Stator current FFT: 50% resistive unbalance,  $J/10$ , 1665 rpm

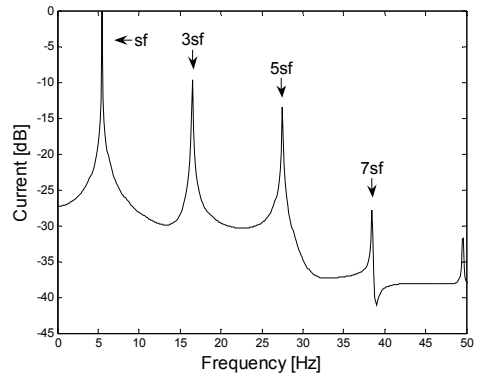


Fig. 12 Rotor current FFT: 50% resistive unbalance,  $J/10$ , 1665 rpm

is proportional to the intensity of the introduced rotor electrical asymmetry itself.

Finally, the model was used to compute the unbalanced machine stator current spectrum for DFIG operation with two different values of rotational inertia. In the first case rotor inertia was set as equal to half its rated value  $J = 0.4/2 \text{ Kgm}^2$  (Fig. 9). The inertia was then decreased by a factor of ten, i.e.  $J = 0.4/10 \text{ Kgm}^2$  (Fig. 10). Rotor unbalance is set as 50% resistive and the speed ripple effect is taken into account in the model calculations. The data in Fig. 9-10 show clearly that inertia has a significant effect on the sideband components in the current spectrum. Compared to the current spectrum given in Fig. 5 for the identical operating conditions and a rated inertia value, where a single pair of sidebands is detectable on each of the identified three "carriers" in the spectrum (i.e. 39, 61, 272, 294, 372 and 394 Hz), the data shown in Fig. 9 for a 50% reduced rotational inertia indicate that the number of detectable sidebands, as well as their respective magnitude, has risen. Now more sideband pairs are detectable on each of the identified "carrier" frequencies, and harmonic components can be identified at 28, 39, 61, 72, 261, 272, 294, 305, 361, 372, 394, 405 and 416 Hz. The current spectrum for a tenfold inertia decrease shown in Fig. 10 confirms this trend and demonstrates a further increase in the number of detectable sideband components throughout the spectrum - their frequencies are labelled in the graph. The magnitude of the calculated asymmetry induced sidebands is seen to be inversely proportional to the inertia value, as is typical of standard cage rotor machines [8]. The rotational inertia influence is further illustrated by model results for the speed and rotor current frequency spectra shown in Fig. 11 and 12, respectively. This data correspond to DFIG operation with a tenfold decrease in rotational inertia value (Fig. 10). The speed ripple harmonics seen in Fig. 11 are also inversely proportional to the inertia and have therefore increased in magnitude with inertia decrease. A resulting sequence of harmonic components with decaying magnitudes is present in the speed signal at  $2sf$ ,  $4sf$ ,  $6sf$  etc. These speed ripple harmonics are ultimately reflected in the rotor current spectrum at  $sf$ ,  $3sf$ ,  $5sf$  etc, as seen in model results in Fig. 12.

## 5 Conclusions

A detailed investigation of DFIG steady-state current frequency spectrum content when machine is operating with a rotor electrical unbalance was performed. The presented results demonstrate that a DFIG rotor asymmetry gives rise to sideband components not only around the fundamental in the stator current spectrum, but also around the higher frequency components found in the spectrum of a balanced machine. The number/detectability of these asymmetry induced sideband frequencies is shown to be strongly affected by speed ripple and rotational inertia, as well as the unbalance intensity. It was also shown that the rotor supply unbalance and the rotor winding unbalance exhibit a compatible influence on the DFIG stator current spectrum content in

terms of the presence of sideband harmonic components.

## Acknowledgements

The authors gratefully acknowledge the funding from the UK EPSRC Supergen Wind Energy Technologies programme, EP/D034566/1.

## References

- [1] Q.F. Lu, Z.T. Cao, E. Ritchie, "Model of stator inter-turn short circuit fault in doubly-fed induction generators for wind turbine", *35th Annual IEEE PESC*, Vol. 2, pp. 932-937, June 2004.
- [2] H. Douglas, P. Pillay, P. Barendse, "The detection of inter-turn stator faults in doubly-fed induction generators", *IEEE Ind. App. Conf.*, Vol. 2, pp. 1097-1102, October 2002.
- [3] D. Shah, S. Nandi, P. Neti, "Stator inter-turn fault detection of doubly-fed induction generators using rotor current and search coil voltage signature analysis", *IEEE Ind. App. Conf.*, pp. 1948-1953, September 2007.
- [4] A. Stefani, A. Yazidi, C. Rossi, F. Filippetti, D. Casadei, G.A. Capolino, "Doubly Fed Induction Machines Diagnosis based on Signature Analysis of Rotor Modulating Signals", *IEEE Trans. on Ind. App.*, Vol. 44, No. 6, pp. 1711-1721, 2008.
- [5] S. Williamson, S. Djurović, "Origins of Stator Current Spectra in DFIGs with Winding Faults and Excitation Asymmetries", *Proc. of IEEE IEMDC 2009 Miami*, pp. 563-570, May 2009.
- [6] S. Nandi, H.A. Toliyat, Xiadong Li, "Condition monitoring and fault diagnosis of electrical motors - a review", *IEEE Trans. on En. Conv.*, Vol. 20, Issue 4, pp. 719-729, Dec. 2005.
- [7] W.T. Thomson, M. Fenger, "Current signature analysis to detect induction motor faults", *IEEE Ind. Appl. Mag.*, Vol. 7, No. 4, pp. 26-34, July/Aug 2001.
- [8] F. Filippetti, G. Francheschini, C. Tassoni, P. Vas, "AI techniques in induction machines diagnosis including the speed ripple effect", *IEEE Trans. on Ind. App.*, Vol. 34, No. 1, January/February 1998.
- [9] C. Kral, F. Pirker, G. Pascoli, "The impact of inertia on rotor fault effects - theoretical aspects of the Vienna monitoring method", *IEEE Trans. on Pow. Elec.*, Vol. 23, no. 4, pp. 2136-2142, July 2008.
- [10] S. Djurović, S. Williamson, A. Renfrew, "Dynamic model for doubly-fed induction generators with unbalanced excitation, both with and without winding faults", *IET Electric Power Applications*, Volume 3, Issue 3, pp.171-177, May 2009.
- [11] S. Djurović, S. Williamson, "A coupled circuit model for a DFIG operating under unbalanced conditions", *IEEE Int. Conf. on Elec. Mach. ICEM*, pp. 1-6, September 2008.
- [12] S. Djurović, S. Williamson, "Losses and pulsating torques in DFIGs with unbalanced stator and rotor excitation", *IEEE ICSET*, pp. 328-333, November 2008.